Lithium−Sodium Metazirconate Solid Solutions, $Li_{2-x}Na_xZrO_3$ ($0 \leq x \leq 2$): A Hierarchical Architecture

Heriberto Pfeiffer,* Enrique Lima, and Pedro Bosch

Instituto de Investigaciones en Materiales, Universidad Nacional Autónoma de México, Circuito exterior s/n, Ciudad Universitaria, Apartado Postal 70-360, Coyoacán, CP 04510, México D.F., Mexico

Received January 13, 2006. Revised Manuscript Received March 23, 2006

Solid solutions of lithium and sodium metazirconates, $Li_{2-x}Na_xZrO_3$ ($0 \leq x \leq 2$), were prepared by coprecipitation. Then, samples were characterized by powder X-ray diffraction, small-angle X-ray scattering, transmission electron microscopy, solid-state nuclear magnetic resonance, and N_2 adsorption (BET). Results show that the solubility limits of sodium into Li_2ZrO_3 and lithium into Na_2ZrO_3 are definitely different. While the maximum amount of sodium that can be inserted into $Li_{2-x}Na_xZrO_3$ is 0.2, the amount of soluble lithium into $Na_{2-x}Li_xZrO_3$ is 0.6. Furthermore, the analyses strongly suggest that $Li_{2-x}Na_xZrO_3$ encloses $Na_{2-x}Li_xZrO_3$, as in a cherry model, and the internal phase is lithium enriched, as shown by the fractal dimension values. The core size is close to 10−20 nm, and the full particle is about 1 μm. The outer shell presents some microporosity. Such a model is supported by kinetic and thermodynamic data.

Introduction

In past decades a wide variety of methods to separate or eliminate polluted gases have been reported. Some of them are based on gas sorption, as carbon dioxide (CO_2), on solid materials such as polymeric membranes, zeolites, soda lime, or on some metal oxides.[1−6] Nowadays, CO_2 elimination from air is one of the most important points established by the Kyoto protocol.[7]

In 1998, Nakagawa and Ohashi reported a novel method to capture CO_2 from high-temperature gases.[8] They proposed CO_2 separation using Li_2ZrO_3, which produces Li_2CO_3 and ZrO_2 at high temperatures (400−600 °C). Later, because CO_2 can be extracted, thermally or chemically, these compounds are recyclable. Since the publication of this article, several studies have been published using lithium ceramics such as Li_2ZrO_3, $Li_6Zr_2O_7$, and Li_4SiO_4.[1,7,9−12] Alternatively, López-Ortiz and co-workers showed that sodium ceramics (Na_2ZrO_3, Na_2TiO_3, and Na_3SbO_4) absorb CO_2 as well. Furthermore, Na_2ZrO_3 presented a better CO_2 sorption than Li_2ZrO_3.[13]

The efficiency of Li_2ZrO_3 and Na_2ZrO_3 has been correlated to the mobility of lithium or sodium in the ceramic skeleton, constituted by $(ZrO_3)^{2-}$ chains. Diffusion of sodium or lithium is determined by the structure and the morphology of the compounds. Although both zirconates have the same elemental stoichiometry (M_2ZrO_3, where M = Li or Na), their crystalline structure is not the same. The Li_2ZrO_3 structure turns out to be more packed than the Na_2ZrO_3 structure (Figure 1). Actually, Na_2ZrO_3 has a lamellar structure, where sodium atoms are located among the $(ZrO_3)^{2-}$ layers. On the contrary, lithium atoms in the Li_2ZrO_3 structure are located in narrow channels. These channels allow lithium movement, but the insertion of sodium in those channels must be, of course, harder than the intercalation of lithium among the Na_2ZrO_3 layers. Hence, mixed compounds Li_2ZrO_3−Na_2ZrO_3 could present original behaviors in CO_2 sorption. The structure of these oxides, $Li_{2-x}Na_xZrO_3$, has not been reported nor has their reactivity in CO_2 sorption. The aim of the present work is to study the synthesis of such compounds and characterize them, systematically. In a future study the CO_2 retention will be presented.

Experimental Section

Zirconates were prepared by coprecipitation. Stoichiometric amounts of lithium carbonate (Li_2CO_3), sodium carbonate (Na_2CO_3), and zirconium acetate ($Zr(OCH_3)_4$) were mixed and dissolved to obtain the solid solution $Li_{2-x}Na_xZrO_3$, where x = 0, 0.2, 0.4, 0.6, 1.0, 1.4, 1.6, 1.8, and 2. Actually, these nominal values were used to label the samples, for example $Li_{1.8}Na_{0.2}ZrO_3$. Each solution was stirred in water for 2 h. Then, the solution was heated at 70

* To whom correspondence should be addressed. Telephone: +52 (55) 5622 4627. Fax: +52 (55) 5616 1371. E-mail: pfeiffer@iim.unam.mx.

(1) Ida, J. I.; Lin, Y. S. *Environ. Sci. Technol.* **2003**, *37*, 1999−2004.
(2) Ding, Y.; Alpay, E. *Process Saf. Environ. Prot.* **2001**, *70*, 45−51.
(3) Baltrusaitis, J.; Grassian, V. H. *J. Phys. Chem. B* **2005**, *109*, 12227−12230.
(4) Iyer, M. V.; Gupta, H.; Sakadjian, B. B.; Fan, L. S. *Ind. Eng. Chem. Res.* **2004**, *43*, 3939−3947.
(5) Macario, A.; Katovic, A.; Giordano, G.; Iucolano, F.; Caputo, D. *Microporous Mesoporous Mater.* **2005**, *81*, 139−147.
(6) Yong, Z.; Rodríguez, A. E. *Energy Convers. Manage.* **2002**, *43*, 1865−1876.
(7) Kato, M.; Yoshikawa, S.; Nakagawa, K. *J. Mater. Sci. Lett.* **2002**, *21*, 485−487.
(8) Nakagawa, K.; Ohashi, T. *J. Electrochem. Soc.* **1998**, *145*, 1344−1346.
(9) Pfeiffer, H.; Bosch, P. *Chem. Mater.* **2005**, *17*, 1704−1710.
(10) Xiong, R.; Ida, J. I.; Lin, Y. S. *Chem. Eng. Sci.* **2003**, *58*, 4377−4385.
(11) Nair, B. N.; Yamaguchi, T.; Kawamura, H.; Nakao, S. I.; Nakagawa, K. *J. Am. Ceram. Soc.* **2004**, *87*, 68−74.
(12) Ida, J. I.; Xiong, R.; Lin, Y. S. *Sep. Purif. Technol.* **2004**, *36*, 41−51.
(13) López-Ortiz, A.; Perez-Rivera, N. G.; Reyes-Rojas, A.; Lardizabal-Gutierrez, D. *Sep. Sci. Technol.* **2004**, *39*, 3559−3572.

10.1021/cm0600935 CCC: $33.50
Published on Web 04/28/2006

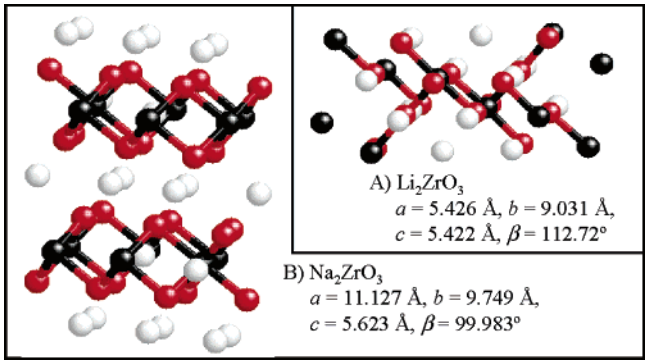

Figure 1. Snapshots of Li_2ZrO_3 and Na_2ZrO_3 structures. The spheres represent, from the brightest to the darkest, the alkaline element (Li or Na), oxygen, and zirconium atoms, respectively.

°C until the precipitate dried. Finally, the powders were heat treated at 900 °C for 4 h.

The samples were characterized by X-ray diffraction (XRD), small-angle X-ray scattering (SAXS), solid-state nuclear magnetic resonance (NMR), transmission electron microscopy (TEM), and nitrogen adsorption (BET).

To obtain the X-ray diffraction patterns, a diffractometer (Bruker AXS, D8 Advance) coupled to a copper anode X-ray tube was used. The relative percentages of the various compounds, identified by the corresponding JCPDS files (Joint Committee Powder Diffraction Standards), were estimated from the total area under the most intense diffraction peak for each phase. The estimated experimental error was ±3%. Cell parameters were determined introducing an internal standard, corundum (α-Al_2O_3). The selected peaks for Na_2ZrO_3 were (020), (200), (011), and (−131), while the peaks selected for Li_2ZrO_3 were (020), (200), (021), and (−202).

A Kratky camera coupled to a copper anode X-ray tube was used to obtain the SAXS curves. Intensity $I(h)$ was measured for 9 min to obtain good quality statistics. The SAXS data were processed with the ITP program,[14−18] in which the angular parameter (h) is defined as $h = 4\pi \sin \theta/\lambda$; θ and λ are the X-ray scattering angle and wavelength, respectively. The radius of gyration (R_g) could then be obtained from the slope of the Guinier plot, Log $I(h)$ vs h^2, in the range 1×10^{-3} Å^{-2} < h^2 < 7×10^{-3} Å^{-2}.[19] The small-angle X-ray scattering may be due either to dense particles in a low-density environment or to pores—or low-density inclusions—in a continuous high electron density medium (Babinet principle).

The shape of the scattering objects was estimated from the Kratky plot, i.e., $h^2[I(h)]$ vs h. The shape was determined depending on the Kratky curve shape; for instance, if the curve presented a peak, the pores/particles were known to be bubbles/globular.[20] If a shape can be assumed, the distance distribution function, i.e., the size distribution function, may be calculated.[16] Last, it is often useful to estimate, from the slope of the curve Log $I(h)$ vs Log(h), the fractal dimension of the scattering objects.[21,22] For this study the background obtained with the Porod plot was subtracted from the experimental intensity. The h interval was $0.07 < h < 0.18$ Å^{-1}.

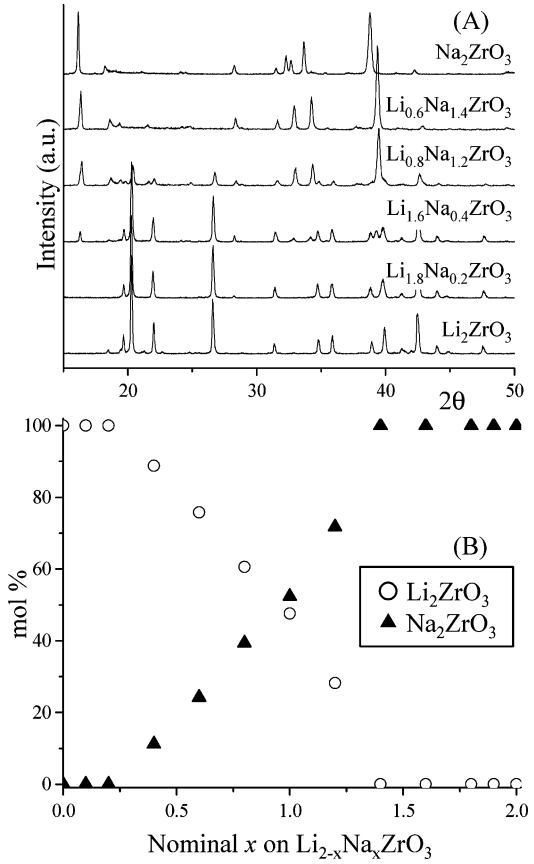

Figure 2. XRD patterns (A) and final composition (B) of different $Li_{2-x}Na_xZrO_3$ solid solutions.

^{7}Li NMR measurements were carried out at room temperature on a Bruker ASX-300 spectrometer (B_0 = 7.05 T, Larmor frequency ν_0 = 116.57 MHz). Single-pulse MAS spectra were obtained using a Bruker MAS probe with a cylindrical 4 mm o.d. rotor. Chemical shifts were referenced to LiCl aqueous solution, and pulse lengths of 2 μs were used. Recycle times were 7 s.

A JEOL JEM-1200EX transmission electron microscope was used to obtain bright field images and electron diffraction patterns. The powder samples were prepared using standard methods.

Surface area analyses were performed on an Autosorb-1 Quantachrome apparatus. The N_2 adsorption isotherms were determined at 77 K by volumetric adsorption. Before the N_2 adsorption process, all the samples (200 mg) were outgassed at 400 °C for 12 h. Surface areas were calculated with the BET equation, and pore diameter values were calculated with the BJH method.

Last, a preliminary CO_2 sorption was performed on the $Li_{1.8}Na_{0.2}ZrO_3$ sample in thermogravimetric equipment (TA Instruments). The sample was heat treated with a heating rate of 5 °C min^{-1} from room temperature to 1000 °C, into a CO_2 flux.

Results

Li_2ZrO_3 (JCPDS file 33-0843) and Na_2ZrO_3 (JCPDS file 35-0770), whose structure is monoclinic, and mixtures of them were obtained using different Li:Na molar ratios. Some of these diffractograms are shown in Figure 2A. Samples with x = 0 and 0.2 only showed the presence of Li_2ZrO_3. Even if the sample contains two phases, the X-ray diffraction patterns will only show the response of the main phase, if the content of one of them is less than 3%. However, if the

(14) Glatter, O. *J. Appl. Crystallogr.* **1981**, *14*, 101−108.
(15) Glatter, O. *J Appl. Crystallogr.* **1988**, *21*, 886−890.
(16) Glatter, O. *Science* **1991**, *84*, 46−54.
(17) Glatter, O.; Hainisch, B. *J. Appl. Crystallogr.* **1984**, *17*, 435−441.
(18) Glatter, O.; Gruber, K. *J. Appl. Crystallogr.* **1993**, *26*, 512−518.
(19) Guinier, A.; Fournet, G. *Small-Angle Scattering of X-rays*; John Wiley & Sons: New York, 1955.
(20) Kataoka, M.; Flanagan, J. M.; Tokunaga, F.; Engelman, D. M. Use of X-ray solution scattering for protein folding study. In *Synchrotron Radiation in the Biosciences*; Chanse, B., Deisenhofer, J., Ebashi, S., Goodhead, D. T., Huxley, H. E., Eds.; Clarendon Press: Oxford, UK, 1994.
(21) Harrison, A. *Fractals in Chemistry*; Oxford University Press: New York, 1995.
(22) Martin, J. E.; Hurd, A. J. *J. Appl. Crystallogr.* **1987**, *20*, 61−78.

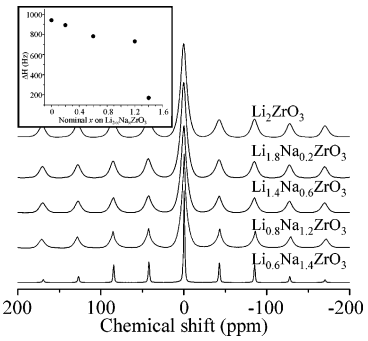

Figure 3. ^{7}Li MAS NMR spectra. The inset represents the broadening of the ^{7}Li peaks as a function of the nominal *x*, on the different zirconates.

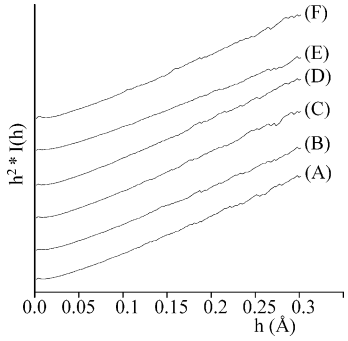

Figure 4. Kratky plots. The shape of the curves is typical of fibrillar pores. (A) Li_2ZrO_3, (B) $Li_{1.8}Na_{0.2}ZrO_3$, (C) $Li_{1.4}Na_{0.6}ZrO_3$, (D) $Li_{0.8}Na_{1.2}ZrO_3$, (E) $Li_{0.6}Na_{1.4}ZrO_3$, and (F) Na_2ZrO_3.

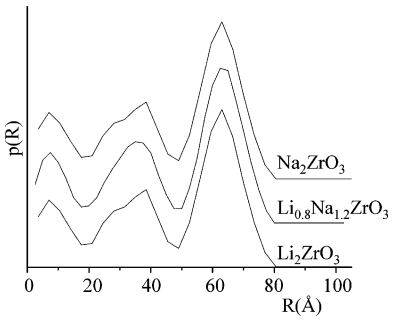

Figure 5. Pore size distributions as determined by SAXS.

x value was increased to 0.4, Na_2ZrO_3 was also found. As the *x* value increased, a mixture of Li_2ZrO_3 and Na_2ZrO_3 was observed. Nevertheless, the Li_2ZrO_3 disappeared when *x* reached 1.4. These results are summarized in Figure 2B.

The solubility limits of sodium into Li_2ZrO_3 and lithium into Na_2ZrO_3 are different, as shown by XRD. While the maximum amount of sodium that could be inserted into $Li_{2-x}Na_xZrO_3$ was 0.2, the amount of soluble lithium into $Na_{2-x}Li_xZrO_3$ was 0.6, 3 times higher. Such a difference may be attributed to the difference in atomic radii of lithium and sodium, 2.05 and 2.23 Å, respectively.[23] Consequently, lithium atoms are expected to diffuse into the Na_2ZrO_3 lattice with more facility than sodium atoms into the Li_2ZrO_3 network. Furthermore, it is favored by the difference in their crystalline structures (Figure 1).

As expected, the ordered inclusion of lithium or sodium expanded or contracted the structure: For example, the (−3,3,1) peak of Na_2ZrO_3 shifted from 38.83° to 39.46° if lithium was incorporated (Figure 2A). The corresponding Na_2ZrO_3 cell parameters decreased, showing that lithium atoms substituted sodium atoms in the crystalline structure. As lithium is smaller than sodium, the system contracted proportionally to the lithium amount, following Vegard's law, up to the $Na_{1.4}Li_{0.6}ZrO_3$ composition. The cell parameters changed from $a = 11.127$ Å, $b = 9.749$ Å, $c = 5.623$ Å, and $\beta = 99.983°$ (Na_2ZrO_3) to $a = 10.93$ Å, $b = 9.51$ Å, $c = 5.52$ Å, and $\beta = 98.02°$ ($Na_{1.4}Li_{0.6}ZrO_3$). The Li_2ZrO_3 cell parameters did not change at all with the insertion of sodium. Hence, sodium atoms may not be substituting lithium into the Li_2ZrO_3 structure. Probably sodium reacted producing very small particles of Na_2ZrO_3 that are beyond the XRD resolution. If that is the case, Na_2ZrO_3 crystallites may be on the surface or occluded into the Li_2ZrO_3 particles.

In all ^{7}Li MAS NMR spectra (Figure 3) only one lithium resonance peak centered at −0.2 ppm was observed. The ^{7}Li spinning sideband (SSB) intensities were very similar in all spectra. Thus, there was only one lithium site in all samples, and this cation is octahedrally coordinated to oxygen atoms. The only significant difference was the line width of the resonances. The noncontaining sodium sample (sample Li_2ZrO_3) presented the broadest peak (936 Hz). In contrast, in the sodium-enriched sample ($Li_{0.6}Na_{1.4}ZrO_3$) the resonance peak was the narrowest (109 Hz).

As ^{7}Li is a quadrupolar nucleus, its resonance is strongly altered by quadrupolar and dipolar interactions, which result in a broadening of the NMR peaks. Hence, in ^{7}Li NMR experiments, the sample without sodium (Li_2ZrO_3) presented the shortest relaxation time value, τ_c, due to spin diffusion by the energy-conserving flip-flop transitions of neighboring ^{7}Li−^{7}Li spin pairs. Therefore, the core lattice corresponding to Na_2ZrO_3 not only incorporates lithium atoms, but it is enriched in the outer shell.

From the SAXS curves, Guinier plots, the gyration radii were found to be 44−45 Å. The difference (1 Å) is not significant as it falls within the error range. The radii of gyration are always calculated without assumptions on the shape of the scattering objects. Still, this shape can be estimated from the Kratky plots (Figure 4) which showed that, independently of the Li content, all samples presented a porous fibrillar shape. Assuming that shape, the size distributions of Figure 5 corresponded to the radii of the scattering particles. The maxima were well resolved and corresponded to 8, 37, and 62 Å.

The plots Log $I(h)$ vs Log(h) are displayed in Figure 6. The linear zones correspond to the fractal dimensions shown in Figure 7. All samples were characterized by a fractal dimension higher than 2.0. The fractal dimension of the pure sodium material might be linked to the lower density and connectivity of that compound. As the material was lithium enriched, the compound became more structured. The corresponding correlation (fractal dimension vs lithium content) turned out to be linear in contrast to R_g (Figure 7).

The morphology of the samples was determined by TEM. Specifically, the sample $LiNaZrO_3$, which contains 48% Li_2ZrO_3 and 52% Na_2ZrO_3, was studied by this technique. Under

(23) Huheey, J. E. *Inorganic Chemistry*, 2nd ed.; Lara J. A.: Mexico City, Mexico, 1981.

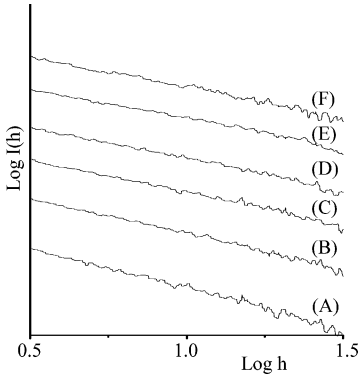

Figure 6. Log $I(h)$ vs Log(h) plots to determine the fractal dimension. (A) Li_2ZrO_3, (B) $Li_{1.8}Na_{0.2}ZrO_3$, (C) $Li_{1.4}Na_{0.6}ZrO_3$, (D) $Li_{0.8}Na_{1.2}ZrO_3$, (E) $Li_{0.6}Na_{1.4}ZrO_3$, and (F) Na_2ZrO_3.

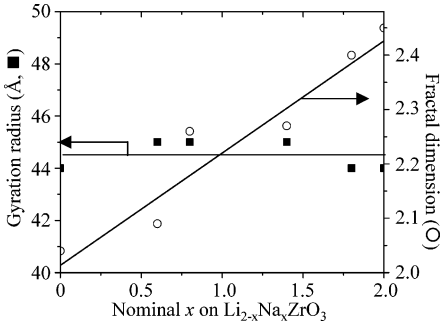

Figure 7. Gyration radius and fractal dimension as a function of nominal x on $Li_{2-x}Na_xZrO_3$.

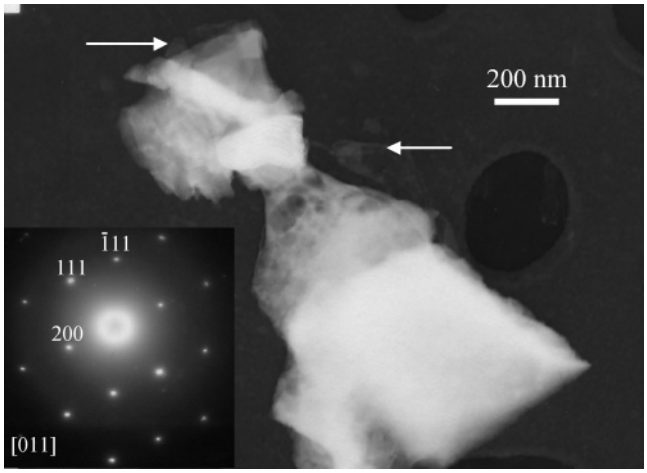

Figure 8. Bright field image and electron diffraction pattern from the sample $LiNaZrO_3$. The arrows indicate residual particles obtained from the outer phase, which was unstable under the electron beam.

the electron beam an outer phase, growing on the surface of a different one, faded out. This outer external compound was almost totally burnt, when the beam was focused on the particle. Instead, the inner compound was much more stable. A bright field TEM image is shown in Figure 8. It was not possible to get a diffraction electron pattern of the external phase. Nevertheless, the electron diffraction pattern of the internal compound showed that it is Na_2ZrO_3. Hence, the external phase must be Li_2ZrO_3.

Besides the morphological information, the particle size was determined. The mean diameter of the particles (Na_2ZrO_3 particles trapped in the Li_2ZrO_3) was around 1 μm. The Na_2ZrO_3 core was around 0.2−0.6 μm, as shown in Figure 8.

Nitrogen isotherms are reported in Figure 9, with their corresponding specific surface areas. Isotherms of Li_2ZrO_3 and $Li_{1.8}Na_{0.2}ZrO_3$ samples were of type III, exhibiting H3 type hysteresis loops, according to the IUPAC classification. This behavior corresponds to aggregates of platy particles. In contrast, isotherms from Na_2ZrO_3-containing samples were type IV, with a H″ type hysteresis loop, which corresponds to structures with interconnected networks of pores of different sizes and shapes. Pore diameter values diminished with sodium content, from 45 to 26 Å up to $x = 0.6$; then pore diameter increased to 47 Å for $x = 2.0$ (Figure 9D).

A preliminary study on CO_2 capture was performed on the $Li_{1.8}Na_{0.2}ZrO_3$ sample. The weight increment was equal to 6.9 wt % at 626 °C, which may be compared to the value obtained in Li_2ZrO_3 of 3−4 wt % at 656 °C reported in the literature.[8]

Discussion

To summarize, from XRD two crystalline compounds were identified, Li_2ZrO_3 and Na_2ZrO_3, where a progressive dilution of lithium into the Na_2ZrO_3 lattice was shown. These measurements are in agreement with the ^{7}Li NMR results. The pore diameter, as determined by N_2 adsorption, decreased as sodium was incorporated up to 0.6 and then grew to 2; the pore diameters decreased from 25 to 13 Å. Transmission electron microscopy suggested a cherry model where Na_2ZrO_3 is in the core of the particles surrounded by Li_2ZrO_3. These values and trends seem to be in disagreement with the SAXS results, which reported homogeneous and larger pores with cylindrical geometry, whose radius was close to 65 Å in all samples. Fractal dimension instead increased with the nominal sodium content.

This apparent contradiction may be explained from the main principles of the techniques. SAXS curves are due to differences in electron densities of inhomogeneities on the materials, in the range of 10−400 Å. In these samples, as sodium atoms have an electron density higher than that of lithium, the frontier between lithium-enriched and sodium-enriched metazirconates should originate the SAXS curves. Therefore, SAXS is sensible to the interface of the materials. Then, the determined fractal dimension has to be understood as a measure of rugosity. As sodium atoms are incorporated, the roughness of the frontier decreases.

It has to be explained that SAXS technique is a bulk technique: Hence, the determined heterogeneity size distributions (Figure 5) correspond to surface porosities as well as to inclusions. They present a peak at 8 Å (radius), which is in agreement with the pore sizes determined by BET. Then, the other values of the distribution obtained by SAXS (37 and 62 Å) should correspond to the bulk. As they are present in all the samples, they must be attributed to building blocks of the M_2ZrO_3 structure, in other words, to the $(ZrO_3)^{2-}$ chains.

Hence, in the proposed cherry model, the external shell is constituted by Li_2ZrO_3. This compound does not incorporate sodium, and the outer surface determines the nitrogen absorption curves. Pore size is the lowest on the $Li_{1.4}Na_{0.6}ZrO_3$ sample; the shell is then continuous around the nucleus. Instead, as sodium content increases, the Li_2ZrO_3 phase is

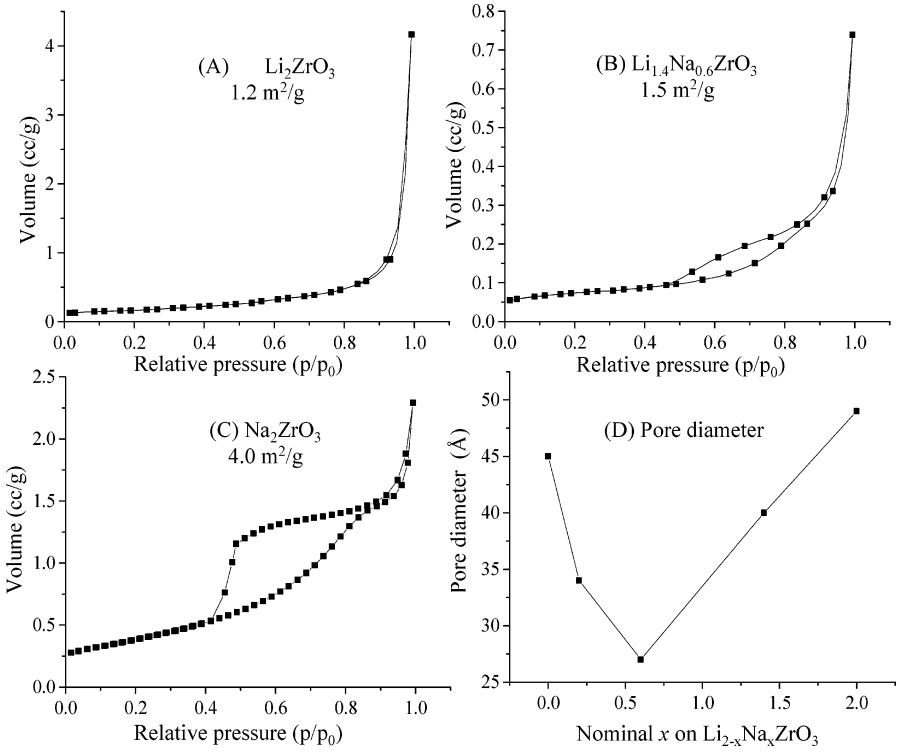

Figure 9. Nitrogen isotherms for different $Li_{2-x}Na_xZrO_3$ samples and their pore diameters.

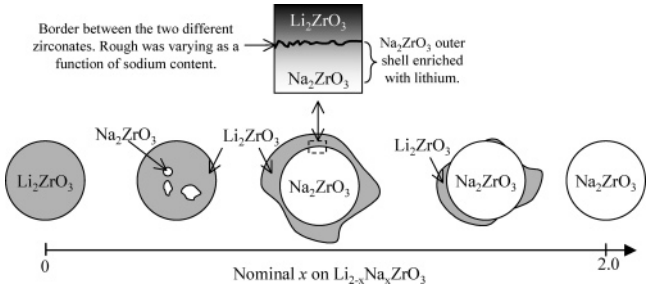

Figure 10. Model of the microscopic composition structure of $Li_{2-x}Na_xZrO_3$ solid solutions as a function of x. The porosity of ceramics is not represented in this model, but it is comparatively different, with Na_2ZrO_3 being more porous than Li_2ZrO_3.

not continuous, and an interparticle porosity is formed as shown by the shape of the nitrogen isotherms.

From those results and discussion, a microscopic composition model is proposed and illustrated in Figure 10. When Li_2ZrO_3 is the main material, it surrounds the Na_2ZrO_3 particles. However, if Na_2ZrO_3 turns out to be the main compound, Li_2ZrO_3 is on the surface, but it cannot cover all the Na_2ZrO_3 particle. Furthermore, in the frontier between zirconates, Na_2ZrO_3 is enriched with lithium on the external part of the core; lithium atoms are scarce in the deeper section of the core. Finally, although porosity is not shown in this scheme, Na_2ZrO_3 is more porous, according to the N_2 adsorption isotherms. Indeed, the isotherm shapes of sodium-containing zirconates suggest that pore shapes are complex and tend to be made up of interconnected networks of pores with different sizes and shapes. Such remarks are not in opposition to the very low surface areas, as gases cannot access this structure. Furthermore, this result confirms that CO_2 cannot penetrate the particles, and lithium and sodium have to diffuse to the surface of the particles.

Last, but not least, the complementary information of the techniques used in this work is as follows. XRD and NMR results gave the composition and crystallographic structure at an atomic level. The interface between zirconates was characterized by the fractal dimension values, and the external surface measured by BET. The full morphology of the mixed oxide particles was obtained by TEM. In this sense, this work determined a hierarchical architecture of the synthesized materials at various levels: Those features should condition absorption and diffusion mechanisms.

The CO_2 retention value obtained with the lowest sodium containing sample, $Li_{1.8}Na_{0.2}ZrO_3$, cannot be explained as a sum of the corresponding retention values of the pure lithium and sodium zirconates (Li_2ZrO_3, 3−4 wt %, and Na_2ZrO_3, 15−17 wt %).[8,13] Therefore, these structural and morphological features are as important as composition. A systematic study is planned to correlate those CO_2 sorption properties.

This chemical behavior and the microscopic model may be justified with kinetic data. The solubility product constants ($k^‡$) are calculated from the Gibbs energies ($\Delta G^‡$) of the substances as solid and those of the aqueous ions at their standard states.[24] Thus for these materials

$$M_2ZrO_3(s) \overset{k}{\leftrightarrow} 2M^+ + (ZrO_3)^{2-}(aq) \qquad (1)$$

where M is Li or Na. Furthermore, as these compounds are extremely insoluble, their $k^‡$, in both ceramics, tend to zero and the values of $k^‡$ cannot be quantified. Besides, solubility depends on $\Delta G^‡$, which is proportional to the formation enthalpy ($\Delta H°_f$). The $\Delta H°_f$ values for Li_2ZrO_3 and Na_2ZrO_3

(24) *CRC Handbook of Chemistry and Physics*, 74rd ed.; Weast, R. C., Astle, M. J., Eds.; CRC: Boca Raton, FL, 1993.

are −1762.3 and −1654.9 kJ mol^{-1}, respectively.[25,26] Hence, this information strongly suggests a higher solubility of Li_2ZrO_3. Furthermore, as the $\Delta H°$ of Na_2ZrO_3 is 107.4 kJ mol^{-1} lower than that of Li_2ZrO_3, Li_2ZrO_3 needs more energy to be produced. In other words, Na_2ZrO_3 is precipitated before Li_2ZrO_3. These thermodynamic data are in good agreement with the model proposed, where Na_2ZrO_3 is in the core of the particles due to its first formation and/or lower solubility, in comparison to Li_2ZrO_3 that is produced afterward, forming a shell around the Na_2ZrO_3 particles.

Conclusions

$Li_{2-x}Na_xZrO_3$ solid solutions ($0 \leq x \leq 2$) were prepared by the precipitation method. The limits of the lithium or sodium solubility into Na_2ZrO_3 and Li_2ZrO_3 were determined by XRD. As lithium is a smaller and lighter atom than sodium, it diffuses into the Na_2ZrO_3. By contrast, sodium did not produce a Na-doped Li_2ZrO_3 solid solution.

The analyses performed by different techniques strongly suggest that lithium phase encloses the sodium phase, as in a cherry model, where the internal interface is lithium enriched. Although BET and SAXS analyses did not seem to concord, each analysis gave different kinds of information. While results of N_2 adsorption correspond to the outer shell, the SAXS analysis gave information on the interface between the two zirconates, as the detection range of this technique is 10−400 Å. These results and the model proposed were supported with kinetic and thermodynamic information, which shows that Na_2ZrO_3 precipitates at shorter times than Li_2ZrO_3, due to its lower solubility.

Acknowledgment. This work was developed in the IMPULSA, UNAM project of Nanotechnology and the ALFA II 0493-FA-FI NANOGASTOR project. The authors thank Dr. J. Chavez-Carvayar for the laboratory facilities, and L. Baños, C. Flores, and V. H. Lara for XRD, TEM, and SAXS, respectively.

CM0600935

(25) Binnewies, M.; Milke, E. *Thermochemical Data of elements and Compounds*, 2nd ed.; Wiley: Weinheim, 2002.
(26) Dash, S.; Sood, D. D.; Prasad, R. *J. Nucl. Mater.* **1996**, *228*, 83−116.